

Chapter 1

Understanding and Applying Single Tip Plasmonics

As discussed in the theoretical background (chapter ??) only a small amount of work has been done to characterise and understand tips prior to applying them as optical nanoantennae. Understanding plasmons in tips, specifically those which can couple with far-field light, has been one of the main motivations of this project. A hyperspectral imaging technique is applied to laterally map light scattering from a tip with confocally localised spectra to infer a local optical response and better study different tips. Understanding this response at the apex of single tips is of importance in determining their effectiveness as near-field enhancers and in understanding their coupling behaviour in the presence of another tip. In this chapter the spectra of single tips is discussed, studying both sharp and spherical-tipped Au AFM probes, along with their application in Raman spectroscopy.

1.1 Optical Characterisation of Nanostructures using Hyperspectral Imaging

Hyperspectral imaging encompasses a range of optical techniques which image using pixels comprised of a spectrum rather than an RGB colour value. This is advantageous over regular imaging as more quantitative information can be extracted from an image. Hence hyperspectral imaging techniques have become commonplace across many diverse fields, including microscopy [1, 2], astrophysics [3], remote sensing and geology [4, 5], food standards [6, 7], and medical imaging [8–10]. Within each of these fields, the features in an image are more clearly identified by their spectral signatures. In this instance, scanning confocal hyperspectral imaging is applied to optically characterise both sharp and nanostructured metallic tips and identify optical resonances originating from localised surface plasmon (LSP) excitation.¹

Scanning confocal hyperspectral imaging falls under the category of spatially scanned imaging. Tips are scanned in a grid under the laser spot and the spectral content of the confocal

¹This technique has also been applied to other periodic, extended nanostructures that are not discussed within the context of this thesis.

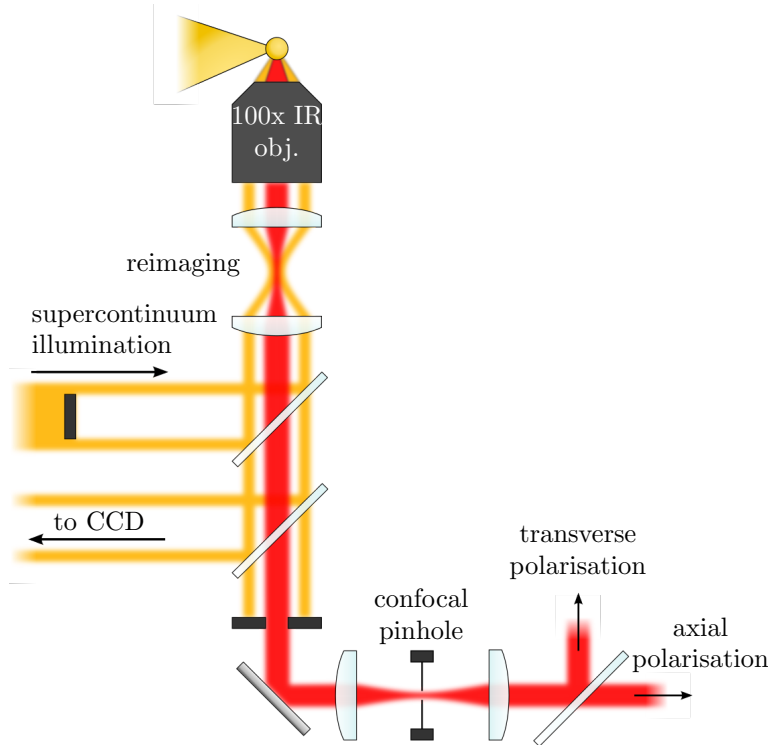


Figure 1.1: Experiment configuration for hyperspectral imaging. The laser is centered on the tip apex for imaging. The tip is scanned across the beam in a grid with spectra acquired at each position. The resulting image then contains 1044 colours at each pixel instead of the usual 3 (RGB).

sampling volume is measured at each point using a spectrometer instead of a photodiode or CCD. Images are then formed at a given wavelength or across a wavelength band. In this instance, using a spectrometer, each image pixel is digitised into 1044 bins between 400–1200 nm rather than the conventional 3 RGB colour bands.² This approach to hyperspectral imaging has previously been used to identify distributed plasmon modes in aggregated AuNP colloids [11] and to image SPPs [12]. By using this technique in the current microscope configuration, as shown in Figure 1.1, LSPs can be spatially identified with sub-diffraction-limited resolutions around 250 nm. Combining it with 80 nm AuNPs also enabled measurement of the microscope PSF and chromatic aberrations, as discussed in chapter ??.

Fast image acquisition is made possible by utilising the ultra-high brightness supercontinuum laser source and sensitive, TE-cooled, benchtop spectrometers with 10–20 ms integration times. Image acquisition is limited only by the integration time at each pixel and the ~30 ms movement time between pixels. The focal intensity is, on average, $\sim 10^5 \text{ W cm}^{-2}$, which is below the damage threshold for 50 nm metallic tip coatings. The illumination and collection configuration is fixed using a preset reference intensity between different samples in order to more quantitatively compare images. Measured spectra of metallic nanostructures are nor-

²The 0.8 nm wavelength resolution of spectra classifies this procedure as hyperspectral, as opposed to multi-spectral imaging in which images are formed using fewer, much broader, wavelength bands.

malised to a BF reflection spectrum of the same flat metal to show structural effects only, such as plasmons.

While not the fastest or most advanced method of acquiring hyperspectral images, spatial scanning is made efficient when used with a supercontinuum white-light source and images benefit from confocal localisation. Other imaging techniques, categorised under “spectral scanning”, “non-scanning” and “spatio-spectral scanning”, have been developed to more efficiently produce hyperspectral images under specific conditions. Spectral scanning involves wide-field imaging through either a range of bandpass filters [13], a tuneable liquid crystal filter [14, 15] or an etalon [16], which is appropriate if studying large areas or if confocal localisation is not required. Similarly, if optical sectioning is not necessary, samples can be imaged with a single direction line scan using an imaging spectrograph (monochromator with CCD) rather than using a two-dimensional grid scan [1]. Non-scanning or snapshot techniques are more complex and computationally demanding than scanning techniques as both spatial and spectral information are acquired in a single static measurement. Imaging is typically achieved using a computed tomography imaging spectrometer (CTIS) [17–20], in which a 2D dispersive grating placed in the Fourier plane results in spectrally separated images on the CCD. Spatio-spectro scanning is the most recent technique, developed in 2014, and involves diagonally scanning through the sample data cube where each point along an axis in the spatial image has a different wavelength [21].

Despite the potential improvements gained by using more advanced hyperspectral imaging techniques, spatial point scanning is deemed the most appropriate solution for tip characterisation, if only for simplicity and compatibility with dual-tip gap spectroscopy. Scan areas are typically small, benefit from confocal localisation, and image acquisition is not time-constrained since the microscope platform is stable.

1.2 Understanding Plasmons in Spherical Nanoparticle Tips

Hyperspectral images are taken of four different types of AFM probes to investigate the plasmonics of nanostuctured tips. AFM tips studied are Au- and Pt-coated standard AFM probes (BudgetSensors Au-coated AFM probes), spherical Au tips (300 nm Au-coated NanoTools B150 AFM probes) [22] and AuNP-on-Pt AFM probes, fabricated in-house using electrochemical deposition [23]. SEM images of a selection of these tips are shown in Figure 1.2. Fabricated tips are pre-treated where possible prior to use with piranha solution to remove organic surface residue and, in some cases, smooth surface roughness.

Comparisons between spherical- and sharp-tipped metallic probes using hyperspectral im-

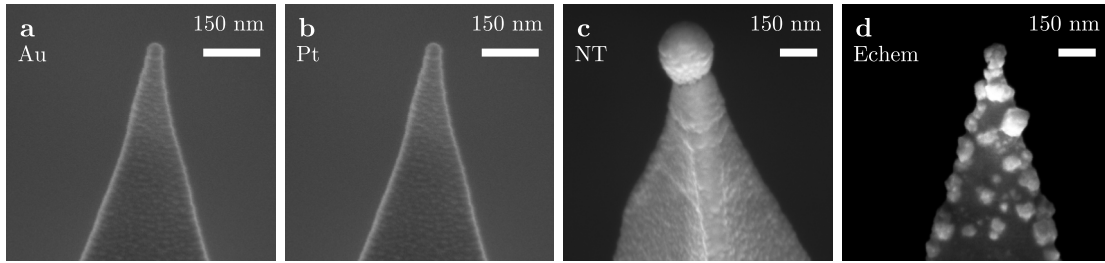


Figure 1.2: SEM images of sharp and spherical metal tips studied using hyperspectral imaging. Tips are (a) a sharp Au AFM tip, (b) a sharp Pt AFM tip, (c) a NT Au-coated spherical AFM tip and (d) an electrochemically deposited AuNP-on-Pt AFM tip.

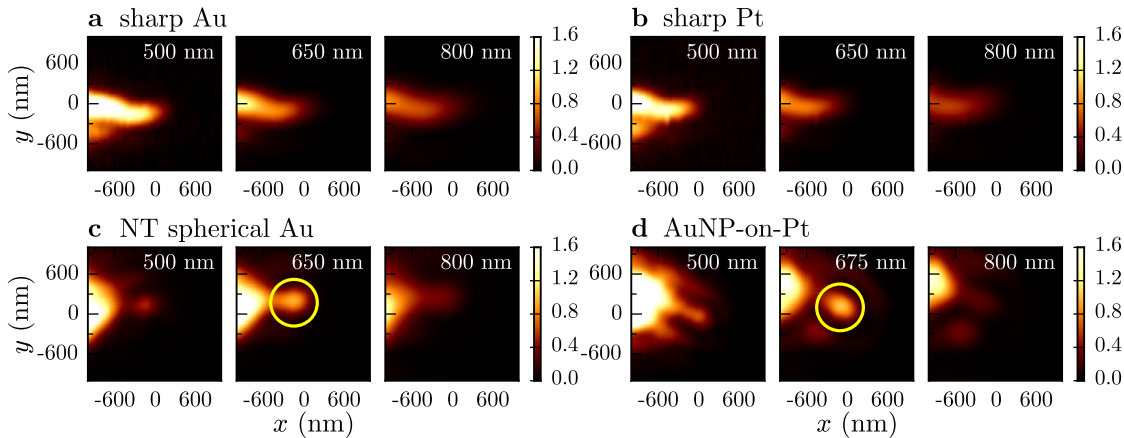


Figure 1.3: Hyperspectral images of sharp and spherical metal tips at wavelengths of interest. Images are of (a) a sharp Au tip, (b) a sharp Pt tip, (c) a NanoTools Au-coated spherical tip and (d) an electrochemically deposited AuNP-on-Pt tip. Collection polarisation is along the tip axis. Colour maps between slices all have the same normalisation. Resonant scattering from spherical apices is clearly seen in the hyperspectral images of between 600–700 nm and highlighted by yellow circles.

age slices (Figure 1.3) show that spherical Au tips exhibit a characteristic red (600–700 nm) scatter, delocalised from the bulk tip. No similar localised scattering is seen for sharp Au or Pt tips in the visible spectrum, which have an overall weaker optical response. This delocalised apex scatter can also be clearly seen in wide-field DF imaging. The AuNP-on-Pt structure behaves very similarly to the Au-coated diamond-like-carbon spherical tip, likely because the 50 nm coating thickness is greater than the skin depth [24, 25]. Plasmons therefore see both as solid Au spheres. Differences in LSPs likely arise due to differences in neck material with Au-Pt and Au-Au neck boundaries.

Integrating spectra around tip apices better shows scattering resonances in spherical Au tips (Figure 1.4a,b), which are reliably present in all spherical-tipped AFM probes, both vacuum-processed and electrochemically deposited. These are attributed to direct LSP excitation. SEM images confirm that this scatter correlates only with spherical Au tip shapes, or when a AuNP is securely attached at the tip apex with a sufficiently small neck joint. The

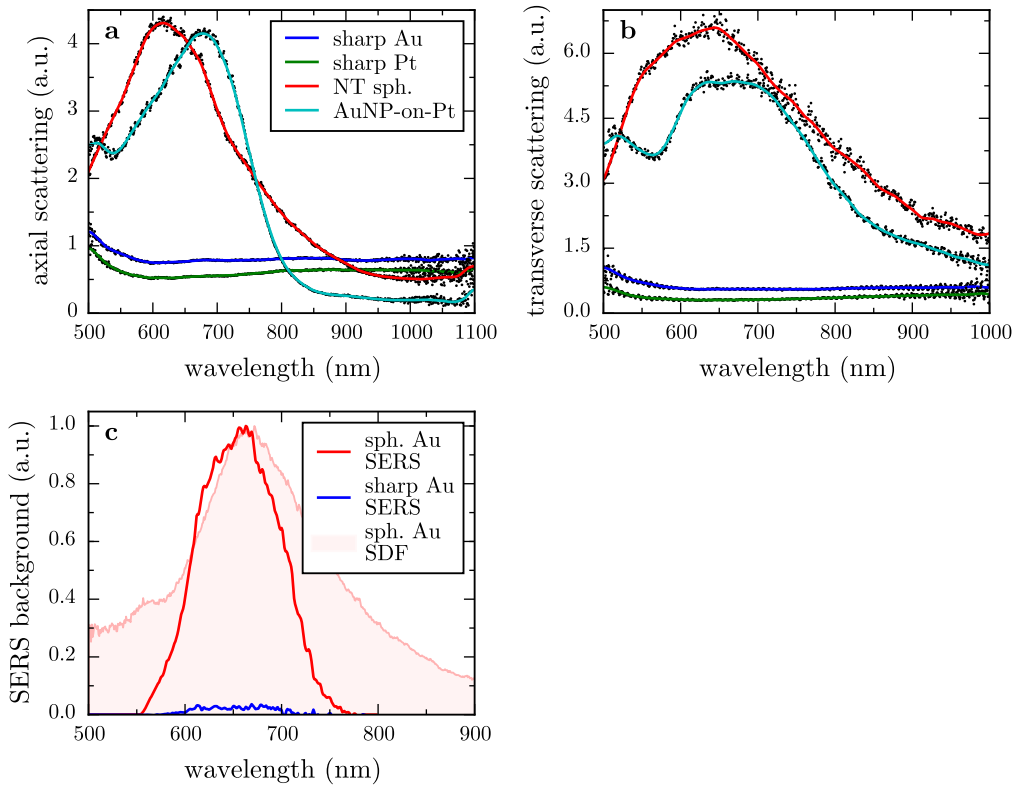


Figure 1.4: Apex spectra of sharp and spherical metal tips. Spectra are extracted from the hyperspectral images in Figure 1.3 by integrating pixels around the apex region in both the axial (a) and transverse (b) polarisations. A clear resonance between 600–700 nm is observed with spherical tips in both polarisations. Sharp metallic tips show comparatively flat spectra. Broadband tuneable SERS background measurements of both a sharp and spherical Au tip are integrated across excitation wavelengths spaced 10 nm apart (c) to confirm excitation of an LSP. Inelastic scattering of light from the tip apex is plasmonically enhanced in the near-field. The background spectrum is the SDF scattering spectrum of the spherical Au tip apex.

response of sharp Au tips shows no similar plasmonic features while the slow rise in scattering towards the NIR is consistent with lightning rod scattering [26].

Broadband tuneable SERS [27] on each of the tips is used to confirm that the resonance is indeed a LSP by showing that the internal near-field is resonantly enhanced.³ During plasmon excitation both internal and external fields are enhanced. The external field leads to strong enhancement of Raman spectra whereas inelastic scatter from electrons inside the metal surface is enhanced by the internal plasmonic field, forming the SERS background [28]. Broadband tuneable SERS is a technique capable of showing both of these components [27]. Hence, the near-field plasmon resonance can be calculated by integrating spectra of the SERS background acquired using a range of excitation wavelengths. SERS background spectra are taken in 10 nm increments of the excitation wavelength and integrated between 500–900 nm. The resulting scattering spectrum, shown in Figure 1.4c, shows a distinct peak around the spherical Au

³Acquisition of broadband tuneable SERS measurements carried out by A. Lombardi.

tip scattering resonance, confirming it as a LSP resonance. Further, confirmation stems from direct observation of plasmon coupling between spherical tips, as has been previously reported [22], with results of the latest tip coupling experiments discussed in detail in the next chapter.

1.2.1 Interpreting the Spectral Response of Metallic Tips

LSPs in spherical Au tips are *radiative* antenna-like modes, similar to those in spherical AuNPs, that can efficiently couple far-field light into strong collective free electron oscillations without the need for SPP momentum matching. As with AuNPs, the signature of these plasmons is a distinct optical resonance indicating their large dipole moment, as seen in Figure 1.4. Such radiative LSPs form only when two close dielectric surfaces surround a metallic particle, allowing for the formation of confined multipolar surface charge oscillations with large dipole moments. Spherical metal tips retain some of the back hemisphere around the connection to the base tip apex (the neck), allowing the spherical apex surfaces to sustain similar plasmons. Sharp tips do not have this back surface, hence cannot support such resonances. Their metal-dielectric surface still, however, supports the launching of evanescent SPPs and a strong lightning rod component.

Partial loss of the backside spherical surface and the introduction of a conductive pathway in spherical tips significantly modifies restoring forces and provides a secondary surface for self-interaction. This makes spherical tips difficult to analytically describe. Numerical simulations of the near-field around spherical tips, computed using BEMAX, are instead employed to better understand their response.⁴

Simulated spectra of the near-field around the apices of 300 nm spherical Au and AuNP-on-Pt tips with 120 nm neck diameters ($d_{\text{neck}} = 0.4d_{\text{sphere}}$) and 20° opening angles are shown

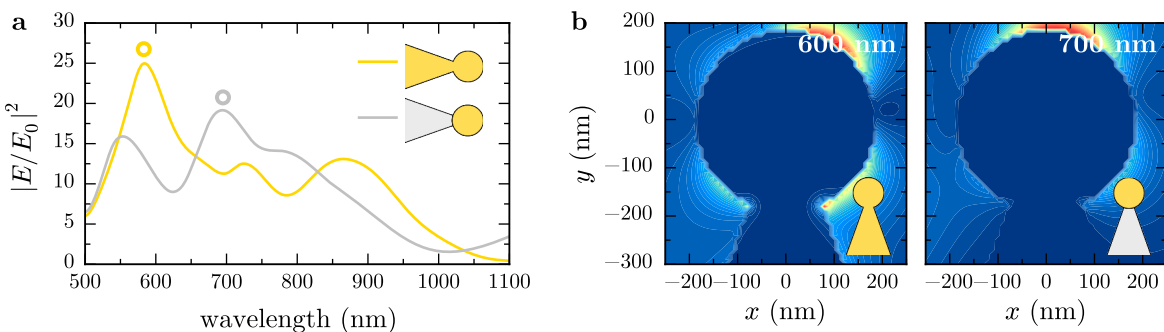


Figure 1.5: Numerical simulations of the field enhancement around a spherical Au tip. (a) Near-field spectra of spherical Au and AuNP-on-Pt tips, extracted from around the apex of the tip. (b) Near-field enhancement distributions of the two resonances highlighted by circles in (a). Simulated tips have a 300 nm spherical radii, 120 nm neck widths, 20° opening angles and 1.88 μm lengths.

⁴BEMAX simulations carried out by D. O. Sigle.

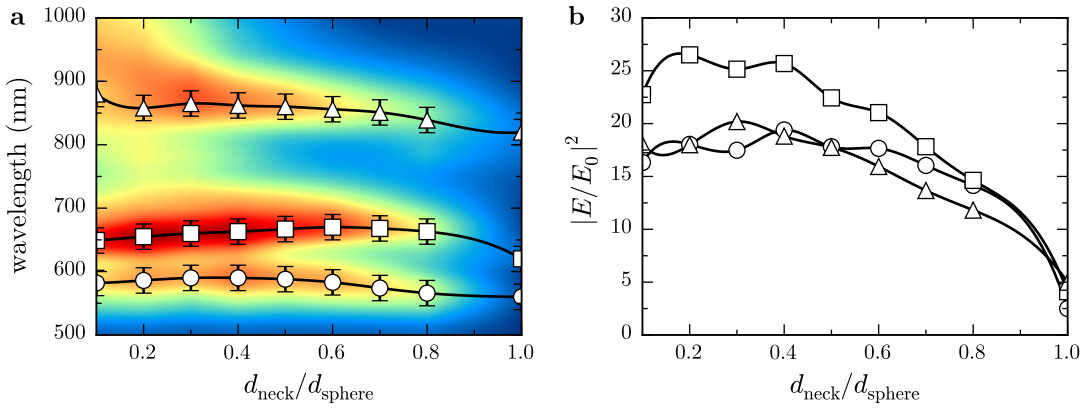


Figure 1.6: Resonant wavelength and field enhancement dependence on the neck width. The resonant wavelength (a) and field enhancement (b) for each of the resonances in spherical Au tips of 250 nm sphere diameter, 1.88 μm length, and 10° opening angle of varying neck widths.

in Figure 1.5a. Tips are simulated with a length of 1.88 μm to avoid truncation artefacts and incident fields are orientated along the tip axis. Strong modes appear for both tips between 550–700 nm similar to experiments. The peak positions of the strongest resonance in each tip approximately agree with experimental spectra. Near-field maps corresponding to the main resonance in each tip are shown in Figure 1.5b. The near-field at the dominant resonance in the spherical Au tip appears more quadrupole-like with a weaker dipole-like resonance occurring above 700 nm. Mie theory shows that visible frequency quadrupolar modes are more favourable in larger AuNPs once dipolar resonances shifts into the NIR. A similarly structured mode to the AuNP quadrupole plasmon would be expected in 300 nm spherical Au tips between 500–600 nm. The neck geometry can potentially short the pole of dipolar plasmons and reduce their confinement, with quadrupolar charge distributions becoming more favourable.

Similar plasmons are found in the AuNP-on-Pt tip except more blueshifted with a 700 nm resonance appearing more dipole-like and a 550 nm resonance appearing more quadrupole-like. Electromagnetic coupling between Au and Pt surfaces is weaker than the interaction between two Au surfaces [29], hence plasmons in the spherical Au tip are less redshifted when attached to a Pt tip apex. The non-plasmonic Pt neck region also forms an additional boundary interface to better confine plasmons to the tip. As a result, the dipole-like mode exists nearer to the visible and becomes more favourable than the quadrupole-like mode and easier to couple to.

In order to directly compare the *plasmonic* behaviour of spherical Au tips with sharp Au tips, independent of the lightning rod contribution, the neck width is incrementally increased. In this manner, the simulated structure transitions from a AuNP attached to the apex of a sharp Au tip into a rounded tip geometry, similar in shape to a sharp Au tip, without the apex radius ever changing. The field enhancement and peak positions extracted from this morphology transition are shown in Figure 1.6. Resonances are insensitive to the neck width until it becomes greater than $0.8d_{\text{sphere}}$ and the tip becomes more similar to sharp tips, ex-

plaining the robustness of observed spherical tip plasmons between different tip morphologies. A steady decrease in the field enhancement, however, is observed once $d_{\text{neck}} > 0.4d_{\text{sphere}}$, decreasing faster once $d_{\text{neck}} > 0.8d_{\text{sphere}}$. This supports the claim that sharp tips cannot sustain antenna-like LSPs.

1.2.2 Implications of Spherical Metallic Tip Plasmonics

The presented results demonstrate importance of considering what plasmons might exist in a particular experiment and nanostructure geometry, and that it is vital to characterise nanostructures prior to their application in any further techniques. Without prior knowledge as to where in the visible spectrum plasmons are excited it is difficult to properly interpret any measurements, such as TERS spectra. Improved tip characterisation is crucial to understanding why such varied TERS enhancements are reported. Standard, wide-field microscopy is not a particularly effective tool for optically characterising tips. Confocal hyperspectral imaging, instead, provides a viable method for mapping the local scattering response with broadband tuneable SERS offering a unique way of optically characterising the near-field.

Exploiting visible LSPs in spherical tips also permits the use of a wider range of illumination configurations as the restriction to evanescent coupling is lifted. Regardless of plasmonics, the lightning rod effect will always play a role in the near-field enhancement process, giving sharp tips an initial advantage, but with careful optimisation of the spherical tip geometry, tips can be brought into resonance with a laser wavelength to maximise enhancement. Spherical Au tips in their current form are already quite well optimised for TERS due to being on resonance with the readily available 633 nm HeNe laser wavelength often used.

Plasmons in spherical tips have also been shown to readily couple with plasmons in other spherical tips [22] and would be expected to couple with image charges in a planar mirror, thus significantly increasing their near-field enhancement. In this situation, their resonances can be tracked as the tip approaches the surface and stopped on resonance with the incident TERS laser for maximum enhancement, for example at the common 785 nm excitation wavelength. For small gaps on the nanometre level, the plasmon mode will become strongly confined to the gap and its contribution to the near-field could outweigh the lightning rod effect. Exploiting radiative tip plasmons in this manner bridges the gap between the plasmonics involved in SERS and TERS. Some of the largest enhancement factors recently measured in plasmonic systems originate from radiative plasmons in AuNPs coupled with their image charge distribution in a mirror [30, 31]. These systems repeatedly produce Raman enhancements of up to 10^7 with nanometric mode volumes, much like tips, demonstrating that plasmonic gaps can exhibit large field enhancement without requiring a significant contribution from the lightning rod effect. However, the static nature of the NPoM geometry lacks the ability to chemically map a surface. By coupling plasmons in spherical tips with their mirror charge, surfaces could be

dynamically mapped with a potentially very large field enhancement.

This discussion on single tip plasmonics is concluded by performing one measurement specifically relevant to TENOM. To demonstrate the advantages of having prior knowledge of excited plasmons in tips, along with the advantages of using AuNP-on-Pt tips, a TERS measurement is performed directly after characterisation on resonance with a plasmon.

1.3 Improved Field Enhancement of Spherical Au Nanoparticle Tips

A result of spherical Au tips sustaining radiative LSPs is that their plasmonic contribution to the field enhancement can outperform the lightning rod contribution in sharp tips (assuming no near-field plasmonic excitation in sharp tips). The field enhancements for both sharp and spherical Au tips, more specifically AuNP-on-Pt tips, are determined in a side illumination configuration using Raman scattering.

SDF spectroscopy is used in conjunction with Raman spectroscopy in a modified version of the microscope platform, enabling both techniques (though not simultaneously). Tips are mounted opposite a second benzenethiol-coated sharp Au AFM tip in a tip-to-tip configuration, mimicking a plasmonic bow-tie antenna (Figure 1.7). This configuration is used to obtain good optical access to the intertip gap for spectroscopically probing its plasmonic properties. Benzenethiol (BTh) is used as a Raman marker for measuring the relative field enhancement of AuNP tips due to its strong Raman response and well-known spectra [32, 33]. BTh (VWR International Thiophenol for synthesis) is diluted to 5 mM solutions in ethanol (Sigma-Aldrich).

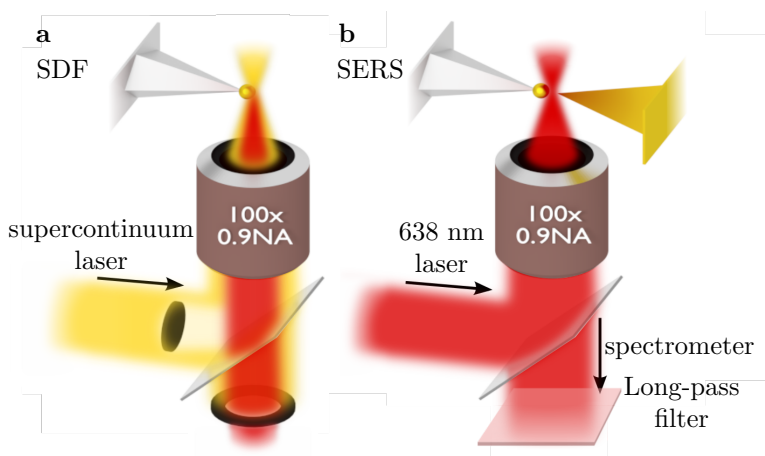


Figure 1.7: Experimental geometry for dark-field spectroscopy and SERS measurements. A 125 nm radius spherical AuNP grown onto a Pt-coated AFM tip is spectroscopically studied using a supercontinuum laser in a dark-field configuration (a). The tip is then brought within 1 nm of a benzenethiol-coated sharp Au tip under 638 nm illumination to measure SERS spectra (b).

A standard Au-coated AFM tip, for use as a SERS substrate, is prepared by coating a monolayer of BTh onto the surface. This is achieved by submerging it in 100 mM ethanolic BTh solution for 1 min followed by rinsing with ethanol and drying in nitrogen. This is repeated 5 times to ensure complete monolayer coverage. Tips used as plasmonic probes are not coated in BTh.

With the BTh tip retracted, a SDF scattering spectrum of the enhancing tip apex is acquired. After characterisation, the microscope optics are modified into a TERS configuration and the enhancing tip is aligned to the BTh tip using the capacitive alignment technique described in chapter ??.⁵ Once aligned, the gap size is reduced to ~ 1 nm, limited by the thickness of the assembled BTh molecular layer, and illuminated through a 100×0.9 NA visible objective with 3 mW (1.9 MW cm^{-2}) of 638 nm laser light incident on the gap, polarised along the tip axis. Scattered light is collected through the same objective and confocally localised. Raman spectra are filtered using a 650 nm long-pass filter (Chroma) prior to dispersion in a spectrometer. Contact dynamics, measured using AFM, confirm that tips come into physical contact while separated by a BTh layer.

Near-field calculations for the spherical Au tip are computed for comparison with experimental results and to understand the enhancement mechanism. The near-field distribution at 633 nm and the spectrum 1 nm from the apex are calculated using the full electrodynamic boundary-element method [34, 35].⁶ The spherical tip is modelled as a Pt cone with half-angle 20° with a 250 nm diameter AuNP attached to its end. The neck diameter between sphere and tip is 100 nm. The tip is illuminated with a plane wave polarised along the tip axis.

A 250 nm diameter spherical AuNP-on-Pt tip, grown as described in chapter ?? (-8 V, 150 ms exposure), is used to demonstrate the augmented plasmonic properties of spherically nanostructured tips. Raman spectra of BTh molecules in the tip dimer gap are greatly enhanced by $30\times$ when using a AuNP tip in place of a sharp Au tip (Figure 1.8a). As the same spectrometer is used for both broadband scattering spectra and SERS spectra, its restricted spectral resolution (300–1100 nm bandwidth), combined with the broadness of the diode laser line illumination, blurs the characteristic multiple Raman peaks of BTh between $1000\text{--}1600 \text{ cm}^{-1}$. However the resulting observation of two broad peaks in this region affirms the presence of BTh in the gap between tips. Absence of an S-H peak around 2200 cm^{-1} suggests good monolayer coverage. The background signal is also enhanced across a broad bandwidth, as is typical for SERS around a plasmon resonance [32].

SDF scattering spectra (Figure 1.8b), taken of individual tips prior to SERS measurements, show that the increased Raman enhancement when using a AuNP tip is due to resonant excitation of a LSP around 630 nm, not present in sharp Au tips. This is in good agreement

⁵The optics are modified in the sense that the laser input is switched, filters are inserted and the dark-field iris is opened.

⁶Near-field calculations carried out by Lars O. Herrmann.

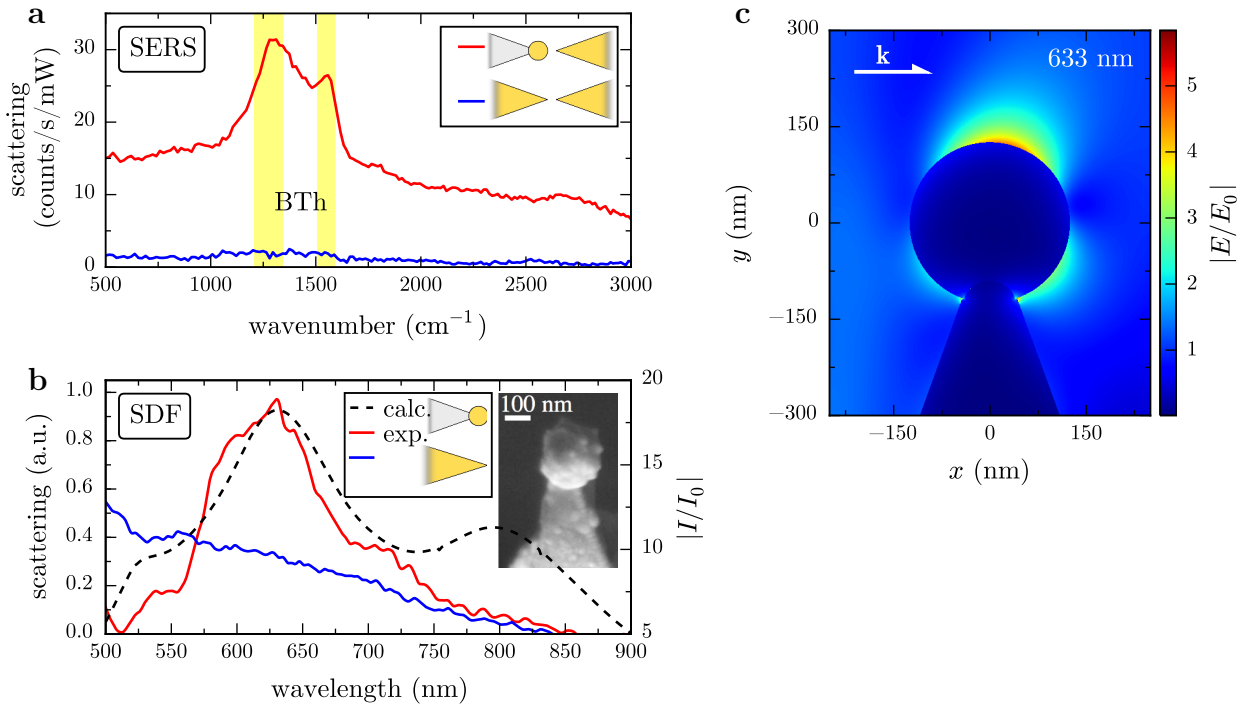


Figure 1.8: Application of sharp Au and AuNP-on-Pt tips to enhancing Raman scattering. (a,b) Comparative TERS and dark-field spectroscopy of sharp Au and AuNP tips. (a) Tip-enhanced Raman spectra of a benzenethiol-coated Au AFM probe brought close to the AuNP tip (red), compared to a sharp Au AFM tip (blue). (b) Dark-field optical scattering of AuNP (red) and sharp Au (blue) AFM tips, with calculated relative intensity enhancement 0.5 nm from the AuNP tip apex (dashed). The inset shows an SEM image of the 250 nm AuNP tip. (c) Calculated field enhancement profile for a 250 nm diameter AuNP at the end of a 1500 nm long Pt tip. The neck join is 50 nm wide and the tip is under longitudinally polarised plane wave illumination at 633 nm.

with boundary element calculations of the near-field enhancement at the AuNP tip apex with a visible plasmon resonance observed across the AuNP (Figure 1.8b,c). Coupling between this LSP in the AuNP tip with a BTh-coated sharp Au tip forms a confined gap plasmon mode. Since coupling is between higher order modes in the sharp Au tip, shifting of this resonance as a function of gap size is weak [36, 37]. A relative SERS enhancement is estimated by taking into account the confinement and mode volume of a LSP in the gap in each case.

LSP mode volumes are estimated using a cylindrical gap mode model. The lateral width of a gap plasmon mode is calculated using $w = \sqrt{R_{\text{eff}}d}$, where R_{eff} is the effective radius of the particles, $\sqrt{R_1 R_2}$, comprising the plasmonic dimer and d is the width of the gap separating particles [38].⁷ This results in lateral mode widths of 4.5 nm for the sharp Au tip of 20 nm radius and 7.1 nm for the 125 nm radius AuNP tip.⁸ Assuming a cylindrical gap mode yields mode volumes of 15.7 nm³ and 39.3 nm³, respectively. These define the near-field contribution

⁷The use of $R_{\text{eff}} = \sqrt{R_1 R_2}$ is justified by...

⁸Note that these widths are below the quantum limit for such large AuNPs, presented in [22], only because the opposing tip has such a small radius to increase localisation.

to Raman scattering and a relative field enhancement is obtained using,

$$FE_{\text{rel}} = \frac{N_{\text{AuNP}}/V_{\text{AuNP}}}{N_{\text{tip}}/V_{\text{tip}}} \quad (1.1)$$

where N is the Raman signal counts and V is the mode volume. This evaluates to a relative SERS enhancement of 12. Since the LSP is laterally confined to only 7 nm within this gap the enhanced Raman signal is the result of scattering contributions from only a very small number of molecules. Lower limit absolute Raman enhancements are estimated using,

$$FE_{\text{abs}} = \frac{N_{nf}/V_{nf}}{N_{ff}/V_{ff}} \quad (1.2)$$

where N_{ff} , the number of counts obtained using only far-field laser light, is assumed to be 0.1 counts/s/mW from the noise levels since signals are below the signal to noise level and V_{ff} is assumed to be 25 000 nm³ based upon the surface of a conical tip exposed to the focal volume of a diffraction limited spot ($d = 412$ nm at $\lambda = 638$ nm). This expression yields absolute, lower-bound Raman enhancements of 1.9×10^5 for a 250 nm AuNP tip and 1.6×10^4 for a sharp Au tip. Though absolute estimates are not as high as the expected 10^7 – 10^8 enhancements reported in the literature [39], the relative SERS enhancement observed with the AuNP tip is indeed comparable to previously reported results [40].

These optical measurements confirm that AuNP tips provide increased field enhancement compared to sharp Au tips due to a strong LSP excitation. Lack of any strong peaks around 600 nm in dark-field spectra of sharp Au tips suggests that any plasmons present are weakly coupled and do not scatter strongly in this illumination geometry, resulting in a lower observed field enhancement. On the other hand, AuNP tips are well suited to high enhancements when illuminated at the appropriate plasmonic resonances. Whilst a number of plasmonic probes have been developed recently, several useful features are obtained here. By using standard AFM probes as a basis, these AuNP tips maintain their functionality as AFM probes for force microscopy. The metallic coating of these tips also allows for simultaneous electrical measurements whilst performing optical and AFM force measurements. These tips therefore function as standard electrical AFM probes with added plasmonic functionality. Furthermore, such tips also show excellent resistance to damage at the tip apex after multiple surface contacts, though surfaces do become deformed after heavy use. Their robust nature is attributed to the direct growth of the AuNP root across the pyramidal tip end. This is a significant improvement over currently-available commercial spherical AFM tips, in which spheres break from the tip and adhere to the contact surface after only one or a small number of contact cycles. All of this is beneficial for creating a dynamically controllable plasmonic dimer on which to perform measurements in the quantum regime. Further applications of spherical

metallic tips can be envisaged, for instance in plasmonic optical trapping [41] because the tips in the present geometry can conveniently act as a heat sink reducing the problematic optical heating observed, and resulting thermal damage.

1.4 Conclusions

Within this chapter it has been shown that spherical AuNP-tipped AFM probes are capable of supporting radiative LSPs in the red part of the visible spectrum that are not supported by the more conventional, sharp Au tips. These plasmons are clearly observed to exist at the apex of extended tip microstructures using scanning confocal hyperspectral imaging in the SDF microscope platform to locally probe the optical response. Broadband tuneable SERS is used to further confirm plasmonic behaviour in spherical Au tips. These techniques are ones that enables plasmon-dependent applications, such as TERS, to pre-screen nanostructured tips to better improve their reliability and reproducibility. The development of antenna-like plasmons in tips through nanostructuring, which readily couple to light without the need for momentum matching, is a step forward for TENOM. Furthermore, these modes determine what plasmonic phenomena are able to be experimentally observed, hence spherical tips can be used to dynamically investigate plasmonics.

References

- [1] R. A. Schultz et al., *Cytometry* **43**, 239–247 (2001).
- [2] S. J. Leavesley et al., *Journal of biophotonics* **5**, 67–84 (2012).
- [3] E. K. Hege et al., in *Optical science and technology*, spie’s 48th annual meeting (International Society for Optics and Photonics, 2004), pp. 380–391.
- [4] J. A. Hackwell et al., in *Spie’s 1996 international symposium on optical science, engineering, and instrumentation* (International Society for Optics and Photonics, 1996), pp. 102–107.
- [5] G. A. Shaw and H.-h. K. Burke, *Lincoln Laboratory Journal* **14**, 3–28 (2003).
- [6] M. Kim, Y. Chen, P. Mehl, et al., *Transactions-American Society of Agricultural Engineers* **44**, 721–730 (2001).
- [7] A. Gowen et al., *Trends in Food Science & Technology* **18**, 590–598 (2007).
- [8] T. Vo-Dinh, *Engineering in Medicine and Biology Magazine, IEEE* **23**, 40–49 (2004).
- [9] M. E. Martin et al., *Annals of biomedical engineering* **34**, 1061–1068 (2006).
- [10] G. Lu and B. Fei, *Journal of biomedical optics* **19**, 010901–010901 (2014).
- [11] L. Herrmann et al., *Optics express* **21**, 32377–32385 (2013).
- [12] M. Bashevoy et al., *Optics express* **15**, 11313–11320 (2007).
- [13] M. Iga et al., *Review of Scientific Instruments* **83**, 103707 (2012).
- [14] R. W. Slawson, Z. Ninkov, and E. P. Horch, *Publications of the Astronomical Society of the Pacific* **111**, 621–626 (1999).
- [15] N. Gat, in *Aerosense 2000* (International Society for Optics and Photonics, 2000), pp. 50–64.
- [16] J. T. Daly et al., in *Symposium on integrated optoelectronics* (International Society for Optics and Photonics, 2000), pp. 104–115.
- [17] T. Okamoto and I. Yamaguchi, *Optics letters* **16**, 1277–1279 (1991).
- [18] T. V. Bulygin and G. N. Vishnyakov, in *Analytical methods for optical tomography* (International Society for Optics and Photonics, 1992), pp. 315–322.
- [19] T. Okamoto, A. Takahashi, and I. Yamaguchi, *Applied Spectroscopy* **47**, 1198–1202 (1993).
- [20] M. Descour and E. Dereniak, *Applied Optics* **34**, 4817–4826 (1995).
- [21] S. Grusche, *Applied optics* **53**, 4594–4603 (2014).

- [22] K. J. Savage et al., *Nature* **491**, 574–577 (2012).
- [23] A. Sanders et al., *Particle & Particle Systems Characterization* **32**, 182–187 (2015).
- [24] M. I. Stockman, *Optics express* **19**, 22029–22106 (2011).
- [25] C. Huber et al., *Physical Chemistry Chemical Physics* **16**, 2289–2296 (2014).
- [26] W. Zhang, X. Cui, and O. J. Martin, *Journal of Raman Spectroscopy* **40**, 1338–1342 (2009).
- [27] A. Lombardi and L. Weller, in preparation (2015).
- [28] J. T. Hugall and J. J. Baumberg, *Physical Review Letters* (2015).
- [29] B. Ren, G. Picardi, and B. Pettinger, *Review of Scientific Instruments* **75**, 837–841 (2004).
- [30] J. Mertens et al., *Nano letters* **13**, 5033–5038 (2013).
- [31] R. W. Taylor et al., *Scientific reports* **4** (2014).
- [32] S. Mahajan et al., *The Journal of Physical Chemistry C* **114**, 7242–7250 (2009).
- [33] P. V. Dudin, P. R. Unwin, and J. V. Macpherson, *The Journal of Physical Chemistry C* **114**, 13241–13248 (2010).
- [34] F. G. De Abajo and J Aizpurua, *Physical Review B* **56**, 15873 (1997).
- [35] F. G. de Abajo and A Howie, *Physical Review B* **65**, 115418 (2002).
- [36] A. Downes, D. Salter, and A. Elfick, *The Journal of Physical Chemistry B* **110**, 6692–6698 (2006).
- [37] J. T. Hugall, J. J. Baumberg, and S. Mahajan, *The Journal of Physical Chemistry C* **116**, 6184–6190 (2012).
- [38] I. Romero et al., *Optics Express* **14**, 9988–9999 (2006).
- [39] B. Pettinger et al., *Annual review of physical chemistry* **63**, 379–399 (2012).
- [40] T. Umakoshi et al., *Applied Physics Express* **5**, 052001 (2012).
- [41] N. C. Lindquist et al., *Laser & Photonics Reviews* **7**, 453–477 (2013).